HHS Public Access

Author manuscript

ACS Appl Mater Interfaces. Author manuscript; available in PMC 2021 May 13.

Published in final edited form as:

ACS Appl Mater Interfaces. 2020 May 13; 12(19): 21210–21220. doi:10.1021/acsami.9b19726.

Iron Magnetic Nanoparticle-Induced ROS Generation from Catechol-Containing Microgel for Environmental and Biomedical Applications

Zhongtian Zhang[1], **Xin He**[2], **Chao Zhou**[3], **Max Raume**[1], **Ming Wu**[2], **Bo Liu**[*,1], **Bruce P. Lee**[*,1]

[1]Department of Biomedical Engineering, Michigan Technological University, Houghton, 49931, USA

[2]School of Environmental Science and Engineering, Guangdong University of Technology, Guangzhou, 510006, China

[3]Institute of Biomedical Engineering and Health Sciences, Changzhou University, Changzhou, 213164, China

Abstract

Reactive oxygen species (ROS) can degrade organic compounds and function as a broad-spectrum disinfectant. Here, dopamine methacrylamide (DMA) was used to prepare catechol-containing microgels, which can release ROS via metal-catechol interaction. A combination of the microgel and iron magnetic nanoparticle (FeMNP) significantly reduced the concentration of four organic dyes (Alizarin Red S, Rhodamine B, Crystal Violet, and Malachite Green) and an antibiotic drug, ciprofloxacin, dissolved in solution. Degradation of dye occurred across a wide range of pH levels (pH 3–9). This simple combination was also antimicrobial against both *Escherichia coli* and *Staphylococcus aureus*. Electron paramagnetic resonance spectroscopy (EPR) results indicate that singlet oxygen was generated during the reaction between catechol and FeMNP at both pH 3 and 7.4, which was responsible for the degradation of organic compounds and bactericidal features of the microgel. Unlike autoxidation that only occurs at a neutral to basic pH, FeMNP-induced catechol oxidation generated singlet oxygen over a wide range of pH level. Additionally, catechol chelates heavy metal ions, resulted in their removal from solution and repurposed these metal ions for dye degradation. This multifunctional microgel can potentially be used for environmental applications for the removal of organic pollutants and heavy metal ions from wastewater, as well as reducing bacterial infection in biomedical applications.

Graphical Abstrct

[*]Corresponding authors: Bruce P. Lee, bplee@mtu.edu, Bo Liu, lbb1107@126.com.

Author Contributions

BPL, BL and ZZ conceived the idea, designed the experiments, and wrote the manuscript. ZZ, XH, MW, CZ, BL, and MR performed experiments. All authors contributed to data analysis and manuscript editing. BPL supervised the whole project.

The authors declare no competing financial interest.

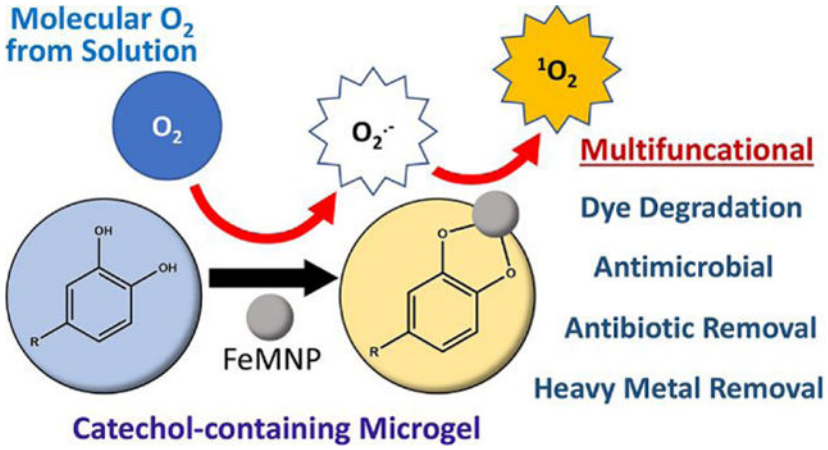

Keywords

Reactive oxygen species; singlet oxygen; catechol; iron magnetic nanoparticle; dye degradation; antimicrobial property

Introduction

Water contamination is a worldwide issue as a result of both rapid population and industrial growth. Wastewater from industries contains organic dyes[1], heavy metal ions[2], and antibiotics[3] which are hazardous to the human health. Moreover, organic compounds from wastewater are rich in nitrogen and phosphorus nutrients, which can result in an overwhelming growth of microorganisms in water[4–5]. Contaminations stemmed from wastewater reduce the availability of drinking water, especially in areas with limited water resources[6]. To alleviate the release of the pollutants into the environment, many significant efforts have been devoted to treating environmental contaminants before they are released. Starting many decades ago, researchers have been seeking solutions for wastewater treatment and bacterial inhibition. Among the various solutions, the use of reactive oxygen species (ROS) have gained interests from the researchers because ROS can degrade organic compounds as well as suppress bacterial growth. ROS include oxygen free radicals and any other oxygen-containing molecule in which an oxygen atom has a greater reactivity than molecular oxygen (O_2)[7]. The high reactivity allows ROS to withdraw electrons from organic compounds, which leads to the degradation of these compounds into water and carbon dioxide[8–10]. Such reactivity from ROS can also cause the death of microorganisms by damaging their cell membrane[11]. Most importantly, ROS degrades into benign degradation products, such as oxygen and water[12].

In order to degrade organic pollutants and kill microorganisms in wastewater with ROS, it is necessary to devise an approach that can generate ROS efficiently. Current approaches in ROS generation include photocatalysis and Fenton's reaction. Photocatalysis applies light as the energy to induce ROS production on a semiconductor-based catalyst[13–15]. Fenton's reaction generates oxygen free radicals from the redox reaction between hydrogen peroxide (H_2O_2) and ferrous ions[9, 16]. However, the application of both approaches described above is

limited by multiple factors. In dye degradation, the efficiency of photocatalysis is restricted to light intensity and the material of the catalyst[17]. Fenton's reaction must be carried out at an acid pH (optimal at pH 3) for an effective ROS generation[9, 18]. Besides these restrictions, both approaches have risks in leaving cytotoxic residuals in water after the process[19–20]. Taking all these issues into consideration, an ROS generation approach which can take place under less-restricted conditions is required for both environmental and biomedical applications.

Catechol is a key functionality that is found in the adhesive proteins used by marine organisms such as mussels[21] and sandcastle worms[22]. ROS can be generated from various catechol oxidation conditions such as autoxidation[23], chemical oxidation[23], and metal-mediated catechol oxidation[24–25]. All these catechol oxidations involve the electron transfer that converts the O_2 into superoxide ($O_2 \cdot^-$) and hydrogen peroxide (H_2O_2) (Scheme 1). Previous publications have reported generation of these ROS during catechol autoxidation[26] and periodate-mediated chemical oxidation[27] (Scheme 1A). The sustained release of H_2O_2 from catechol autoxidation was found to be both antimicrobial and antiviral[28]. However, autoxidation or chemical-induced oxidation of catechol is favored at a neutral to basic pH[26–27]. A recent study suggests that a different ROS, singlet oxygen ($^1O_2$), can be generated via metal ion-mediated catechol oxidation (Scheme 1B)[29]. $^1O_2$ is able to degrade organic dyes and provide antibacterial effects[30–31]. Although the use of metal nanoparticle to induce ROS generation have not been previously reported, we hypothesize that iron-based nanoparticle can potentially be used to generate $^1O_2$ potentially in the same manner as metal ion-mediated catechol oxidation.

Herein, we synthesized microgel using catechol-bearing dopamine methacrylamide (DMA) and mixed the microgel with iron magnetic nanoparticle (FeMNP) (Scheme 2). The efficacy for this simple mixture to degrade organic dyes (Alizarin Red S, Rhodamine B, Crystal Violet, and Malachite Green), remove the antibiotic ciprofloxacin (CIP) from an aqueous solution, and suppressed bacterial growth was examined. Additionally, the ability for DMA-containing microgel to remove heavy metal ion from an aqueous solution and repurpose the metal ion for dye degradation was also explored. Finally, the type of ROS that is generated during FeMNP-induced catechol oxidation was determined using electron paramagnetic resonance (EPR) spectroscopy.

Experimental Methods

Materials

N-Hydroxyethyl acrylamide (HEAA), TWEEN®80, Span™80, acetone, FeMNP (97% iron oxide (Fe_3O_4); 50–100 nm particle size), potassium hexacyanoferrate (II) trihydrate, nickel (II) nitrate hexahydrate, copper (II) nitrate hemi(pentahydrate), cobalt (II) chloride hexahydrate, lead (II) nitrate, Alizarin Red S, Rhodamine B, Crystal Violet, Malachite Green, ciprofloxacin, 5,5-dimethylpyrroline N-oxide (DMPO) and 2,2,6,6-Tetramethylpiperidine (TEMP) were purchased from Sigma Aldrich (St Louis, MO). Methylene bis-acrylamide (MBAA) was purchased from Acros Organics (Fair Lawn, New Jersey). VA-086 was purchased from Wako Chemicals (Richmond, VA). Dimethyl sulfoxide (DMSO) and hexanes were purchased from VWR (Radnor, PA). L13152 LIVE/DEAD®

BacLight™ Bacterial Viability Kit and Pierce™ Quantitative Peroxide (FOX) Assay Kit were purchase from Thermo Fisher Scientific (Waltham, MA). *Staphylococcus aureus* and *Escherichia coli* were purchased from ATCC (Manassas, VA). Dopamine methacrylamide (DMA, Figure S1) was synthesized following published protocols[32].

Preparation of DMA-containing microgels

Microgels were prepared by following previously published protocol with some minor modifications[28]. 70 mL of hexanes, 500 μL of Span™80, and 100 μL of TWEEN®80 were mixed and stirred vigorously in a rubber plug-sealed flask under a nitrogen-rich atmosphere for 15 min. Polymer precursor solutions were prepared by mixing 1 M of HEAA with 0–40 mol% of DMA, 6 mol% of MBAA, and 4 mol% of VA086 (increased to 12 mol% of VA086 for 40 mol% of DMA) relative to HEAA in DMSO and DI water (DMSO:DI water volume ratio = 2:2.48). The precursor solutions were frozen for 30 min and degassed 3 times by back filling with N_2. Then, the precursor solutions were added to the surfactant mixture drop by drop using a syringe. The reaction was initiated by irradiating UV light (365 nm, UVP UVGL-25, Analytik Jena) with continued stirring at 1400 RPM for 4 h 30 min. The microgels were washed and centrifuged sequentially with acetone, isopropyl alcohol, acetone, and DI water until the microgels became white. The microgels were lyophilized to yield dried microgel powder.

The composition of the microgels were analyzed using Fourier-transform infrared (FTIR) spectroscopy (Spectrum One, PerkinElmer Instruments, CT) with Attenuated Total Reflection (ATR) accessory. The morphology of dried microgel was visualized using field emission scanning electron microscope (FESEM, Hitachi S-4700, Hitachi High Technologies America, Inc., IL). The morphology of the swollen microgels was studied under a light microscope after incubating the samples in DI water for 30 min. Particle size of the microgel in the dried and swollen states were determined from the microscope images with ImageJ.

Dye degradation experiments

2.5–10 mg of FeMNP and 25 mg of microgel were incubated in up to 150 mg/mL of different dye solutions (pH 3–9) containing either Alizarin Red S, Rhodamine B, Crystal Violet, or Malachite Green at 37 °C for up to 24 hours. After incubation for a given amount of time, 200 μL of the solution was diluted 15 times and examined using UV-vis spectroscopy (LAMBDA35, PerkinElmer, MA). Standard curves of each dye (Figure S2) was used to determine the residual dye concentration in the solution. The repeatability of microgel in dye degradation was examined. 40 mol% DMA microgel and 5 mg/mL of FeMNP were incubated with Rhodamine B for 24 hours and collected using vacuum filtration. Then, the microgel and FeMNP mixture was washed with water (pH 3) and acetone and lyophilized before incubating with Rhodamine B again.

Antibiotic removal experiment

5 mg of FeMNP and 25 mg of microgel were incubated a solution (pH 7.4) containing up to 0.45 mM of ciprofloxacin. The concentration of ciprofloxacin in the solution was examined

using UV-vis spectroscopy. A standard curve of ciprofloxacin (Figure S3) was used to determine the residual ciprofloxacin concentration in the solution.

Heavy metal ion absorption

Solution containing 5–40 mM of metal ions was prepared by dissolving different metallic salts (e.g., potassium hexacyanoferrate (II) trihydrate, nickel (II) nitrate hexahydrate, copper (II) nitrate hemi(pentahydrate), cobalt (II) chloride hexahydrate, and lead (II) nitrate) in an aqueous solution acidified to pH 3 using HCl. 25 mg of microgel was incubated with 1 mL of solution containing the metal ions at room temperature for 24 hours. After which, microgels were collected and dried under vacuum. The solutions were tested under inductively coupled plasma optical emission spectrometry (ICP-OES, Optima 7000DV, PerkinElmer, MA) to determine the amount of residual metal ion concentration in the solution. The dried microgels were coated with platinum (thickness = 20 nm), imaged under an environmental scanning electron microscope (ESEM, XL 40, FEI/Philips, OR) and mapped using energy-dispersive X-ray spectroscopy (EDS). To determine the effect of soluble metal ions on dye degradation, 25 mg of microgel and 0.02 mmol of different metallic compounds were added to 1 mL Rhodamine B solution (150 mg/L, pH 3) and incubated at 37 °C for 24 hours. The concentration of the residual dye in the solution was determined using UV-vis spectroscopy as described above.

Antibacterial activity of DMA microgel and FeMNP

40 mol% DMA microgels and FeMNP were added into 24-well tissue culture plates and sterilized using UV irradiation for 2 hours. The antibacterial activity of the microgels was evaluated following published protocols with minor modifications[28]. Both *S. aureus* and *E. coli* grown on the stock plate were diluted by broth to a concentration of 100,000 CFU/mL. the sterilized microgels (10 mg) and FeMNP (2 mg) were equilibrated with 225 mL of PBS (pH 7.4) for 5 min. 500 mL of bacteria suspended in broth solution was added to the microgel, and the mixture was incubated at 37 °C. At a given time point (4, 8, and 24 hours), a 1-mL loop was immersed into the mixture without touching the precipitated microgels and streaked onto agar plates, which were further incubated at 37 °C for 24 hours. The agar plates with colonies were photographed, and the bacteria colonies were counted using ImageJ. The relative colony number was calculated following the equation below:

$$\text{Relative colony number} = (1 - N_m/N_c) \times 100\%$$

where N_m is the colony numbers formed from the bacteria exposed to the microgels and N_c is the average colony numbers formed from the bacteria cultured in broth that did not contain any microgel.

2 mL of bacteria suspension was seeded onto a glass confocal dish for 24 h at 37 °C. The sterilized microgels (25 mg) and FeMNP (5 mg) were added and further incubated for another 24 h at 37 °C. The microgels and FeMNP were removed and the glass dish was stained using L13152 LIVE/DEAD® BacLight™ Bacterial Viability according to the manufacturer's protocol and examined using a fluorescence microscope (LSM710, Zeiss,

Germany). Fluorescence imaging was performed with a 480/500 nm filter for SYTO 9 stain and 490/635 nm filter for propidium iodide in the microscope optical path.

Determination of ROS generation

Electron paramagnetic resonance (EPR) spectroscopy was used to determine the free radicals generated by DMA-containing microgels. 25 mg of 40 mol% DMA microgel and 5 mg FeMNP were added to 4 mL of aqueous solution (either pH 3 or pH 7.4) mixed with 1 mL of methanol and 12.4 μL of DMPO to determine the generation of hydroxyl radical (·OH) and $O_2{\cdot}^-$. To determine the generation of $^1O_2$, 12 μL of 14 mM of TEMP was prepared and then was added into the mixture containing 40 mol% DMA microgel (25 mg/mL), FeMNP (5 mg/mL) and 4 mL of aqueous solution (pH 3 or 7.4). EPR spectra were obtained immediately after the mixing using an EPR spectrometer (EMX Plus, Bruker, MA). H_2O_2 generation from microgels was determined using FOX Assay Kit by following a published protocol using a Synergy Mx microplate reader (BioTek, VT)[28]. The conversion of superoxide to singlet oxygen in the presence of FeMNP was confirmed by mixing 12 μL of 14 mM of TEMP and 5 mg of FeMNP to 1 mL of 250 mg/mL potassium superoxide dissolved in anhydrous DMSO.

Statistical Analysis

One-way analysis of variance (ANOVA) and student t-test were performed for comparing means of multiple groups and two groups, respectively, using a p-value of 0.05.

Results and Discussions

FTIR spectra of the microgels confirm the presence of features associated with HEAA (620 and 1053 cm^{-1} for −OH, 1547 cm^{-1} for amide, 1628 cm^{-1} for C=O, and 2934 and 1440 cm^{-1} for $-CH_2-$) (Figure 1). Microgels containing 20 and 40 mol% of DMA exhibited new peaks at 800 and 1250 cm^{-1} (aromatic C-H bending)[33], which confirms the presence of catechol in the microgels. These microgels appeared spherical in shape when visualize in both dried and wet conditions (Figure 2). The particle size ranged from 25 to 54 μm when dried (Table S1). After the hydration, the microgels increased in size (51–67 μm) and retained the spherical shape. The addition of DMA decreased the overall hydrophilicity of the crosslinked microgels, which likely resulted in the smaller size of the DMA-containing microgels when compared to the 0 mol% DMA microgel. Additionally, catechol can participate in hydrogen bonding and π-π interaction[25], which also contributed to the deswelling as observed in a previous publication[28].

Organic compound degradation and removal

The ability of the combination of DMA-containing microgel with FeMNP to degrade organic dyes was examined using four different dyes: Alizarin Red S, Rhodamine B, Crystal Violet, and Malachite Green (Figure 3). These dyes were incubated with microgels containing 0–40 mol % of DMA and FeMNP. In general, there was a significant higher reduction in dye concentration when incubated with microgels with increasing DMA content (Figure 3A and Figure S4–7). Apart from Alizarin Red S (17% of original dye concentration remained), the dye concentrations of Rhodamine B, Crystal Violet, and Malachite Green

were significantly reduced to less than 1 % of their original concentrations after 24-hour incubation with 40 mol% DMA microgel and FeMNP. These values are equivalent to or are approaching values that were reported for photocatalyzed (99–100% reduction)[34–36] and Fenton's reaction-mediated (94–99% reduction)[37–39] dye degradation. The solutions containing these different colored dyes became colorless after incubation with DMA microgel and FeMNP, which indicated the breakdown of these organic dye compounds (Figure 3B). Microgels that did not contain DMA also resulted in a smaller amount of reduction in dye concentration (2–66% reduction), potentially due to the dye being absorbed into the microgel network. However, the presence of catechol was required to achieve greater than 99% dye reduction. In the absence of FeMNP, the 40 mol% DMA microgels reduced dye concentration (24–81% reduction) through absorption, potentially due to the π-π interaction between the aromatic structures of the dyes and catechol. The concentrations of the untreated dyes did not change over the same period indicating that they were stable during the incubation.

Among the dyes tested, Rhodamine B demonstrated the least reduction as a result of physical absorption (2% reduction using 0% DMA microgel) but still achieved greater than 99 % dye reduction using 40 mol% DMA microgel. This indicated that Rhodamine B was predominantly degraded through ROS generated by catechol. As such, a series of experiments was performed to further study the dye degradation behavior using Rhodamine B as the model compound under different conditions. The initial Rhodamine B concentration was varied between 0.3 to 6 mM (144 to 2880 mg/mL). 40 mol% DMA microgel and FeMNP effectively degraded more than 99 % of Rhodamine B over 24 hours for initial dye concentration up to 3 mM (Figure 3C). At the highest dye concentration tested (6 mM), the percentage of dye reduction was significantly lowered (~20% reduction). The 40 mol% DMA microgel and FeMNP combination degraded 99 % of dye over a wide pH range (pH 3 to 9) (Figure 3D). Changing the amount of FeMNP did not influence the dye degradation results (Figure S8). The 40 mol% DMA microgel degraded 99 % of dye at pH 3 with FeMNP concentrations ranging from 2.5 to 10 mg/mL. The dye reduction kinetic study showed that the dye concentration had a rapid decrease within the first 10 minutes after the mixing the dye with the microgel and FeMNP (Figure 3E, Figure S9). Nearly 80% of the dye was degraded within this period. However, the microgel were not recyclable (Figure S10). The recycled microgels did not reduce the dye concentration compared to the original microgels with the presence of FeMNP, potentially due to irreversible oxidation of catechol. However, FeMNP appeared to be tethered to the microgel rendering it magnetic (Figure S11).

Besides the organic dyes, the ability of DMA-containing microgels in combination with FeMNP in removing an antibiotic drug, ciprofloxacin (CIP), was also examined (Figure 4). CIP is an antibiotic drug used the treatment of urinary and digestive infections and pulmonary diseases[40]. The combination of 40 mol% DMA microgel and FeMNP resulted in the lowest residual amount of CIP after 24-hour incubation. For a starting CIP concentration of 0.23 mM or lower, CIP concentrations was reduced to around 1% of its original concentration (99% reduction). At the highest CIP concentration tested (0.45 mM), CIP was reduced by over 91%. In the absence of FeMNP, 40 mol% DMA microgel also reduced CIP concentration in a similar concentration dependent manner (84–99 % reduction). However, 0

mol% DMA microgel only resulted in marginal reduction in CIP concentration (23–25% reduction). The reduction in CIP concentration is an effect of both the adsorption of the CIP by the catechol containing microgel and the ROS generated by the oxidation of catechol. CIP consists of a multi-ringed structure decorated with electron negative elements (Figure S12). It is likely that the presence of catechol aided in CIP absorption into the DMA-containing microgel potentially through π-π interaction and hydrogen bonding. Moreover, previously, it has been reported that CIP can be degraded by ROS such as $O_2{\cdot}^-$ and ·OH[41–42]. In the results, the addition of FeMNP to DMA-containing microgel further reduced CIP concentration, presumably due to ROS-mediated degradation.

Metal ion removal

The ability of the microgels to absorb heavy metal ions was determined by incubating 40 mol% DMA microgel with a solution containing up to 40 mM of various metal ions (Figure 5). DMA microgels removed over 85 % of Fe^{2+}, Ni^{2+}, Cu^{2+}, and Co^{2+} ions and more than 65 % of Pb^{2+} ion from the solution regardless of the initial concentration of metal ion. Microgels that absorbed metal ions such as Fe^{2+} and Cu^{2+} become slightly discolored, changing from the original white color to a yellowish and brownish color (Figure 5B). This an indication that metal ions were removed along with the microgels. SEM images with the utilization of EDS mapping further confirmed that the metal elements were detected on the surface of the microgel (Figure 5C). Catechol's ability to chelate these metal ions aided in their removal. Additionally, the microgel is insoluble and could be easily separated from the solution through filtration or precipitation.

The ability for metal ions to catalyze Rhodamine B in the presence of 40 mol% DMA microgel was further examined. When incubating Rhodamine B with different metal ions (Fe^{2+}, Ni^{2+}, Cu^{2+}, Co^{2+}, Pb^{2+}), there was minimal reduction in dye concentration except Pb^{2+} (6% reduction) (Figure S13A). However, more than 99 % of Rhodamine B was degraded after incubating with 40 mol% DMA microgels and the same series of metal ions (Figure S13B, Figure S14). This result indicated that dye degradation only occurred in the presence of catechol using the metal ion as a catalyst, presumably as a result of $^1O_2$ generation through metal ion-mediated catechol oxidation (Scheme 1B)[29]. DMA-containing microgel not only removed heavy metal ions present in the aqueous solution, it also utilized the metal ion to generate ROS for organic dye degradation.

Antimicrobial properties of DMA microgel with FeMNP

The antimicrobial properties of DMA-containing microgel in combination with FeMNP was evaluated using a Gram-positive (*S. aureus*) and a Gram-negative (*E. coli*) bacteria (Figure 6 and Figure S15). For the untreated control and bacteria incubated only with FeMNP, colony-forming units (CFU) increased with incubation time. This indicated that FeMNP alone has no antimicrobial properties. At each time point, 40 mol% DMA microgel alone effectively killed 91–94 and 91–95% of *S. aureus* and *E. coli*, respectively. DMA-containing microgel generates 5–8 mM of H_2O_2 at pH 7.4 as result of catechol autoxidation (Figure S16), which has been previously demonstrated to be effective against both bacterial strains[28]. Adding FeMNP to DMA-containing microgel resulted in no difference in the antimicrobial property toward *S. aureus*. However, after 24 hours of incubation, the combination of 40 mol% DMA

microgel and FeMNP killed more *E. coli* (99%) when compared to in the absence of FeMNP (91%). This difference in the antimicrobial property may be attributed to different ROS generated in the presence of FeMNP[43]. Varying the FeMNP content (2.5 – 10 mg/mL) did not affect antibacterial results (Figure S17), and a FeMNP concentration as low as 2.5 mg/mL exhibited antimicrobial effect.

Additionally, the antimicrobial ability for the combination of DMA-containing microgel and FeMNP on pre-establish culture of bacteria was examined using LIVE/DEAD fluorescence imaging (Figure 7). In the absence of the microgel and FeMNP, bacteria were stained green indicated live cells. However, when the surfaces seeded with *S. aureus* and *E. coli* were treated with 40 mol% DMA microgel and FeMNP, the bacteria were predominantly killed and stained red (Figures 7B and D, respectively).

Generation of ROS

EPR was used to further examine the types of ROS that were generated when combining DMA-containing microgel with FeMNP using TEMP and DMPO as the capture agents (Figure 8). $^1O_2$ oxidizes TEMP and the oxidized TEMP can be detected using EPR[29]. At both pH 3 and 7.4, a characteristic three-peak pattern appeared when using TEMP as the capture agent, which indicates that $^1O_2$ is generated by DMA-containing microgel and FeMNP (Figures 8A and B). On the other hand, $O_2\cdot^-$ and ·OH can be captured by DMPO[44]. However, there was no signal resulting from adding DMPO (Figures 8C and D), indicating that $O_2\cdot^-$ and ·OH radicals were not generated.

The ability for nanoparticles in inducing ROS generation has been previously reported using gold[45] and copper[46] nanoparticles. However, generation from catechol and a nanoparticle had not been previously described. Recently, Yi et al.[29] reported that $^1O_2$ was generated between catechol and metal ions. Moreover, we successfully detected singlet oxygen in a mixture of potassium superoxide and FeMNP in anhydrous DMSO using EPR (Figure S18). The ability for iron nanoparticle to catalyze $^1O_2$ from $O_2\cdot^-$ has also been reported recently[47]. Inspired by this finding, we propose a mechanism for $^1O_2$ generation between DMA microgel and FeMNP (Figure 9). The oxidation of catechol moiety in DMA-containing microgel is catalyzed by FeMNP, which converts catechol into *o*-semiquinone radicals. At the same time, the electron transfer converts O_2 into $O_2\cdot^-$ during the *o*-semiquinone formation. The *o*-semiquinone radical is stabilized by the interfacial metal-catechol coordination bond formed with the FeMNP surface[48]. Because the *o*-semiquinone radical has been stabilized by FeMNP, electron transfer is preferred between $O_2\cdot^-$ and FeMNP. As a result, FeMNP oxidizes the superoxide radical into $^1O_2$, which is similar to the metal-mediated catechol oxidation (Scheme 1B). No $O_2\cdot^-$ was captured using EPR, further confirming that $O_2\cdot^-$ was rapidly converted to $^1O_2$. FeMNP-catalyzed oxidation process also differs from autoxidation of catechol to generate superoxide (Scheme 1A), which is favored at a neutral to basic pH[26]. We further confirmed that no H_2O_2 production was detected from the DMA microgel at an acidic pH (Figure S19). On the other hand, Fenton's reaction is optimal in an acidic pH[9, 18]. FeMNP was able to oxidize catechol at both an acidic and a basic pH (Figure 8A), which enabled ROS generation capability across a wider range of pH levels (Figure 3D).

When taken together, we investigated the multifunctionality of catechol for the potential in organic compound degradation, heavy metal ion removal, and antimicrobial applications. $^1O_2$ generated by FeMNP-catalyzed oxidation of catechol effectively degraded organic dyes at a level similar to those of photocatalyzed and Fenton's reaction-mediated dye degradation[34–39]. DMA-containing microgel can also be used to remove heavy metal ion and even use the metal ion for dye degradation. Additionally, the generated ROS was effective in killing both Gram-positive and negative bacteria. However, the effectiveness of the generated $^1O_2$ as catalyzed by FeMNP did not improve significantly when compared to the efficacy of those of H_2O_2 generated during autoxidation (i.e., in the absence of FeMNP). This is potentially due to the significantly short half-life of $^1O_2$ (3.5 microsecond[49]) when compared to that of H_2O_2 (8 hours[50]), even though $^1O_2$ is a more potent ROS than H_2O_2[51].

When compared with other ROS generation approaches, DMA-containing micorgel in conjunction with FeMNP converted molecular oxygen present in an aqueous solution into a more reactive $^1O_2$. Even in the absence of FeMNP, DMA-containing micorgel was able to repurpose heavy metal ions present in the solution for ROS generation. In addition, both the microgel and FeMNP are removable. The microgels can be collected with a filter, and the FeMNP can be removed with magnets. Furthermore, strong interaction between catechol and FeMNP resulted in the attachment of FeMNP to DMA-containing microgel and the mixture became magnetic as well (Figure S11). Although FeMNP has been previously found to have environmental applications[52–53], the ability to remove these materials from solution will reduce their environmental impacts. Most importantly, these microgels do not contain hazardous ROS, which is only generated when the microgel is hydrated in an aqueous solution. This material can potentially serve as a lightweight and portable source for on-demand generation of ROS with simple activation and multifunctionality packed into one system.

Conclusions

DMA-containing microgels in combination with FeMNP was demonstrated to degrade and reduce the concentration of organic dyes over a wide range of pH (pH 3–9). The generated ROS degraded CIP and killed over 90 % of *S. aureus* and of *E. coli*. These microgel absorbed remove more than 85 % of various metal ions from solution and repurposed the absorbed metal ions for dye degradation. EPR spectroscopy confirmed that $^1O_2$ was generated when mixing DMA-containing microgel with FeMNP, in a mechanism potentially similar to that of metal ion-induced oxidation of catechol.

Supplementary Material

Refer to Web version on PubMed Central for supplementary material.

ACKNOWLEDGMENT

The authors acknowledge Director Owen Mills and the Applied Chemical & Morphological Analysis Laboratory (ACMAL) at Michigan Technological University for the use of instruments and staff assistance. We also thank Jennifer Eikenberry from the School of Forest Resources and Environmental Science and Wenkai Jia from the Department of Biomedical Engineering for their assistance in ICP-OES analysis and light microscope imaging, respectively.

Funding Sources

The authors acknowledge funding from the National Institutes of Health under Award Nos. R15GM104846 (B.P.L), the Office of Naval Research under Award No. N00014-16-1-2463 (B.P.L), and the Office of the Assistant Secretary of Defense for Health Affairs through the Defense Medical Research and Development Program under Award No. W81XWH1810610 (B.P.L).

REFERENCES

1. Yagub MT; Sen TK; Afroze S; Ang HM Dye and Its Removal from Aqueous Solution by Adsorption: A Review. Advances in colloid and interface science 2014, 209, 172–184. [PubMed: 24780401]
2. Fu F; Wang Q Removal of Heavy Metal Ions from Wastewaters: A Review. Journal of environmental management 2011, 92, 407–418. [PubMed: 21138785]
3. Gothwal R; Shashidhar T Antibiotic Pollution in the Environment: A Review. Clean–Soil, Air, Water 2015, 43, 479–489.
4. Elmgren R; Larsson U Nitrogen and the Baltic Sea: Managing Nitrogen in Relation to Phosphorus. The Scientific World Journal 2001, 1, 371–377. [PubMed: 12805876]
5. Yang S; Yao G Simultaneous Removal of Concentrated Organics, Nitrogen and Phosphorus Nutrients by an Oxygen-Limited Membrane Bioreactor. PloS one 2018, 13, e0202179. [PubMed: 30161154]
6. Kostyla C; Bain R; Cronk R; Bartram J Seasonal Variation of Fecal Contamination in Drinking Water Sources in Developing Countries: A Systematic Review. Science of the Total Environment 2015, 514, 333–343. [PubMed: 25676921]
7. González C; Agapito M; Rocher A; Gonzalez-Martin M; Vega-Agapito V; Gomez-Nino A; Rigual R; Castañeda J; Obeso A Chemoreception in the Context of the General Biology of Ros. Respiratory physiology & neurobiology 2007, 157, 30–44. [PubMed: 17331812]
8. Wang J; Guo Y; Liu B; Jin X; Liu L; Xu R; Kong Y; Wang B Detection and Analysis of Reactive Oxygen Species (Ros) Generated by Nano-Sized Tio2 Powder under Ultrasonic Irradiation and Application in Sonocatalytic Degradation of Organic Dyes. Ultrasonics Sonochemistry 2011, 18, 177–183. [PubMed: 20684888]
9. Babuponnusami A; Muthukumar K A Review on Fenton and Improvements to the Fenton Process for Wastewater Treatment. Journal of Environmental Chemical Engineering 2014, 2, 557–572.
10. Liu G; Zhang Y; Xu L; Xu B; Li F A Pw 12/Bi 2 Wo 6 Composite Photocatalyst for Enhanced Visible Light Photocatalytic Degradation of Organic Dye Pollutants. New Journal of Chemistry 2019, 43, 3469–3475.
11. Su H-L; Chou C-C; Hung D-J; Lin S-H; Pao I-C; Lin J-H; Huang F-L; Dong R-X; Lin J-J The Disruption of Bacterial Membrane Integrity through Ros Generation Induced by Nanohybrids of Silver and Clay. Biomaterials 2009, 30, 5979–5987. [PubMed: 19656561]
12. Scandalios JG The Rise of Ros. Trends in biochemical sciences 2002, 27, 483–486. [PubMed: 12217524]
13. Konstantinou IK; Albanis TA Tio2-Assisted Photocatalytic Degradation of Azo Dyes in Aqueous Solution: Kinetic and Mechanistic Investigations: A Review. Applied Catalysis B: Environmental 2004, 49, 1–14.
14. Ajmal A; Majeed I; Malik RN; Idriss H; Nadeem MA Principles and Mechanisms of Photocatalytic Dye Degradation on Tio 2 Based Photocatalysts: A Comparative Overview. Rsc Advances 2014, 4, 37003–37026.
15. Nosaka Y; Nosaka AY Generation and Detection of Reactive Oxygen Species in Photocatalysis. Chemical reviews 2017, 117, 11302–11336. [PubMed: 28777548]
16. Nidheesh PV; Gandhimathi R; Ramesh ST Degradation of Dyes from Aqueous Solution by Fenton Processes: A Review. *Environmental Science and Pollution Research* 2013, 20, 2099–2132. [PubMed: 23338990]
17. Djurišić AB; Leung YH; Ng AMC Strategies for Improving the Efficiency of Semiconductor Metal Oxide Photocatalysis. Materials Horizons 2014, 1, 400–410.

18. Lin SH; Lo CC Fenton Process for Treatment of Desizing Wastewater. Water research 1997, 31, 2050–2056.
19. Intarasuwan K; Amornpitoksuk P; Suwanboon S; Graidist P Photocatalytic Dye Degradation by Zno Nanoparticles Prepared from X2c2o4 (X= H, Na and Nh4) and the Cytotoxicity of the Treated Dye Solutions. Separation and Purification Technology 2017, 177, 304–312.
20. Chui CH; Man KW; Tsang WF; Lam PL; Leung KSY; Wong WY; Kan CW; Lam KH Study of the Cytotoxicity of Reactive Dyeing Effluent Treated by F Enton Oxidation. Coloration Technology 2013, 129, 398–402.
21. Yu M; Hwang J; Deming TJ Role of L-3, 4-Dihydroxyphenylalanine in Mussel Adhesive Proteins. Journal of the American Chemical Society 1999, 121, 5825–5826.
22. Wang CS; Stewart RJ Multipart Copolyelectrolyte Adhesive of the Sandcastle Worm, Phragmatopoma Californica (Fewkes): Catechol Oxidase Catalyzed Curing through Peptidyl-Dopa. Biomacromolecules 2013, 14, 1607–1617. [PubMed: 23530959]
23. Kalyanaraman B; Felix C; Sealy R Semiquinone Anion Radicals of Catechol (Amine) S, Catechol Estrogens, and Their Metal Ion Complexes. Environmental health perspectives 1985, 64, 185–198. [PubMed: 3007089]
24. Friedrich LC; Machulek A Jr; Silva V. d. O.; Quina FH Interference of Inorganic Ions on Phenol Degradation by the Fenton Reaction. Scientia Agricola 2012, 69, 347–351.
25. Yang J; Stuart MAC; Kamperman M Jack of All Trades: Versatile Catechol Crosslinking Mechanisms. Chemical Society Reviews 2014, 43, 8271–8298. [PubMed: 25231624]
26. Meng H; Li Y; Faust M; Konst S; Lee BP Hydrogen Peroxide Generation and Biocompatibility of Hydrogel-Bound Mussel Adhesive Moiety. Acta biomaterialia 2015, 17, 160–169. [PubMed: 25676582]
27. Meng H; Liu Y; Lee BP Model Polymer System for Investigating the Generation of Hydrogen Peroxide and Its Biological Responses During the Crosslinking of Mussel Adhesive Moiety. Acta Biomater. 2017, 48, 144–56. [PubMed: 27744069]
28. Meng H; Forooshani PK; Joshi PU; Osborne J; Mi X; Meingast C; Pinnaratip R; Kelley J; Narkar A; He W Biomimetic Recyclable Microgels for on-Demand Generation of Hydrogen Peroxide and Antipathogenic Application. Acta biomaterialia 2019, 83, 109–118. [PubMed: 30541699]
29. Yi Q; Ji J; Shen B; Dong C; Liu J; Zhang J; Xing M Singlet Oxygen Triggered by Superoxide Radicals in a Molybdenum Cocatalytic Fenton Reaction with Enhanced Redox Activity in the Environment. Environmental science & technology 2019, 53, 9725–9733. [PubMed: 31331171]
30. Caine MA; McCabe RW; Wang L; Brown RG; Hepworth JD The Influence of Singlet Oxygen in the Fading of Carbonless Copy Paper Primary Dyes on Clays. Dyes and pigments 2001, 49, 135–143.
31. Dahl T; RobertMiddenand W; Hartman P Pure Singlet Oxygen Cytotoxicity for Bacteria. Photochemistry and photobiology 1987, 46, 345–352. [PubMed: 3313445]
32. Lee H; Lee BP; Messersmith PB A Reversible Wet/Dry Adhesive Inspired by Mussels and Geckos. Nature 2007, 448, 338. [PubMed: 17637666]
33. Wang S-H; Griffiths PR Resolution Enhancement of Diffuse Reflectance Ir Spectra of Coals by Fourier Self-Deconvolution: 1. Ch Stretching and Bending Modes. Fuel 1985, 64, 229–236.
34. Rasalingam S; Wu C-M; Koodali RT Modulation of Pore Sizes of Titanium Dioxide Photocatalysts by a Facile Template Free Hydrothermal Synthesis Method: Implications for Photocatalytic Degradation of Rhodamine B. ACS applied materials & interfaces 2015, 7, 4368–4380. [PubMed: 25633643]
35. Sajid MM; Khan SB; Shad NA; Amin N; Zhang Z Visible Light Assisted Photocatalytic Degradation of Crystal Violet Dye and Electrochemical Detection of Ascorbic Acid Using a Bivo 4/Fevo 4 Heterojunction Composite. RSC advances 2018, 8, 23489–23498.
36. Mohamed A; Ghobara MM; Abdelmaksoud M; Mohamed GG A Novel and Highly Efficient Photocatalytic Degradation of Malachite Green Dye Via Surface Modified Polyacrylonitrile Nanofibers/Biogenic Silica Composite Nanofibers. Separation and Purification Technology 2019, 210, 935–942.

37. Xu D; Sun X; Zhao X; Huang L; Qian Y; Tao X; Guo Q Heterogeneous Fenton Degradation of Rhodamine B in Aqueous Solution Using Fe-Loaded Mesoporous Mcm-41 as Catalyst. Water, Air, & Soil Pollution 2018, 229, 317.
38. Idrissi M; Miyah Y; Benjelloun Y; Chaouch M Degradation of Crystal Violet by Heterogeneous Fenton-Like Reaction Using Fe/Clay Catalyst with H2o2. Journal of Materials and Environmental Science 2016, 7, 50–58.
39. Elhalil A; Tounsadi H; Elmoubarki R; Mahjoubi F; Farnane M; Sadiq M; Abdennouri M; Qourzal S; Barka N Factorial Experimental Design for the Optimization of Catalytic Degradation of Malachite Green Dye in Aqueous Solution by Fenton Process. Water Resources and Industry 2016, 15, 41–48.
40. Glassmeyer ST; Furlong ET; Kolpin DW; Cahill JD; Zaugg SD; Werner SL; Meyer MT; Kryak DD Transport of Chemical and Microbial Compounds from Known Wastewater Discharges: Potential for Use as Indicators of Human Fecal Contamination. Environmental Science & Technology 2005, 39, 5157–5169. [PubMed: 16082943]
41. Kumar JV; Karthik R; Chen S-M; Muthuraj V; Karuppiah C Fabrication of Potato-Like Silver Molybdate Microstructures for Photocatalytic Degradation of Chronic Toxicity Ciprofloxacin and Highly Selective Electrochemical Detection of H 2 O 2. Scientific reports 2016, 6, 34149. [PubMed: 27671795]
42. Durán-Álvarez JC; Avella E; Ramírez-Zamora RM; Zanella R Photocatalytic Degradation of Ciprofloxacin Using Mono-(Au, Ag and Cu) and Bi-(Au–Ag and Au–Cu) Metallic Nanoparticles Supported on Tio2 under Uv-C and Simulated Sunlight. Catalysis Today 2016, 266, 175–187.
43. Slavin YN; Asnis J; Häfeli UO; Bach H Metal Nanoparticles: Understanding the Mechanisms Behind Antibacterial Activity. Journal of nanobiotechnology 2017, 15, 65. [PubMed: 28974225]
44. Kalyanaraman B; Felix C; Sealy R Photoionization of Melanin Precursors: An Electron Spin Resonance Investigation Using the Spin Trap 5, 5-Dimethyl-1-Pyrroline-1-Oxide (Dmpo). Photochemistry and Photobiology 1982, 36, 5–12.
45. Hone DC; Walker PI; Evans-Gowing R; FitzGerald S; Beeby A; Chambrier I; Cook MJ; Russell DA Generation of Cytotoxic Singlet Oxygen Via Phthalocyanine-Stabilized Gold Nanoparticles: A Potential Delivery Vehicle for Photodynamic Therapy. Langmuir 2002, 18, 2985–2987.
46. Jose GP; Santra S; Mandal SK; Sengupta TK Singlet Oxygen Mediated DNA Degradation by Copper Nanoparticles: Potential Towards Cytotoxic Effect on Cancer Cells. Journal of nanobiotechnology 2011, 9, 9. [PubMed: 21439072]
47. Yang Z; Qian J; Yu A; Pan B Singlet Oxygen Mediated Iron-Based Fenton-Like Catalysis under Nanoconfinement. Proceedings of the National Academy of Sciences 2019, 116, 6659–6664.
48. Amstad E; Gillich T; Bilecka I; Textor M; Reimhult E Ultrastable Iron Oxide Nanoparticle Colloidal Suspensions Using Dispersants with Catechol-Derived Anchor Groups. Nano Lett. 2009, 9, 4042–4048. [PubMed: 19835370]
49. Ogilby PR Singlet Oxygen: There Is Still Something New under the Sun, and It Is Better Than Ever. Photochemical & Photobiological Sciences 2010, 9, 1543–1560. [PubMed: 20963239]
50. Cooper WJ; Lean DR Hydrogen Peroxide Concentration in a Northern Lake: Photochemical Formation and Diel Variability. Environmental science & technology 1989, 23, 1425–1428.
51. Elstner E Oxygen Radicals—Biochemical Basis for Their Efficacy. Klinische Wochenschrift 1991, 69, 949–956. [PubMed: 1665886]
52. Gutierrez AM; Dziubla TD; Hilt JZ Recent Advances on Iron Oxide Magnetic Nanoparticles as Sorbents of Organic Pollutants in Water and Wastewater Treatment. Reviews on environmental health 2017, 32, 111–117. [PubMed: 28231068]
53. Tang SC; Lo IM Magnetic Nanoparticles: Essential Factors for Sustainable Environmental Applications. Water research 2013, 47, 2613–2632. [PubMed: 23515106]

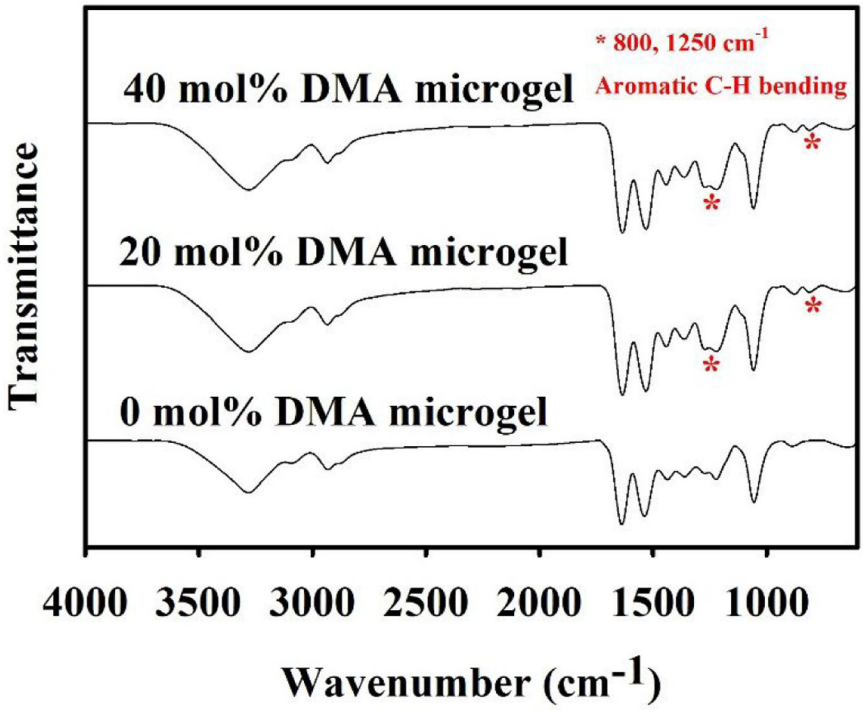

Figure 1.
FTIR spectra of microgels containing 0–40 mol% of DMA. * indicates peaks associated with bending of aromatic C-H bending.

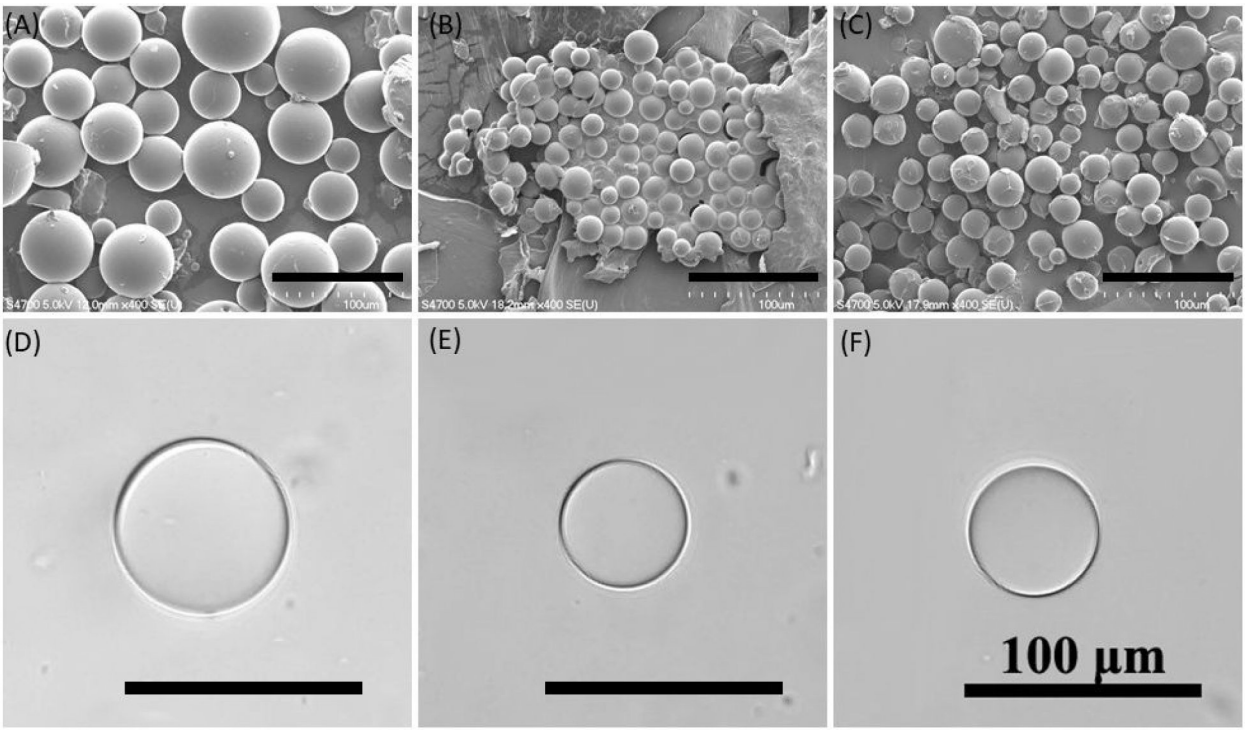

Figure 2.

FE-SEM images of dried microgels containing (A) 0, (B) 20, and (C) 40 mol% of DMA. Images of swollen microgels containing (D) 0, (E) 20, and (F) 40 mol% DMA visualized using a light microscope. Black lines are the scale bars (100 μm).

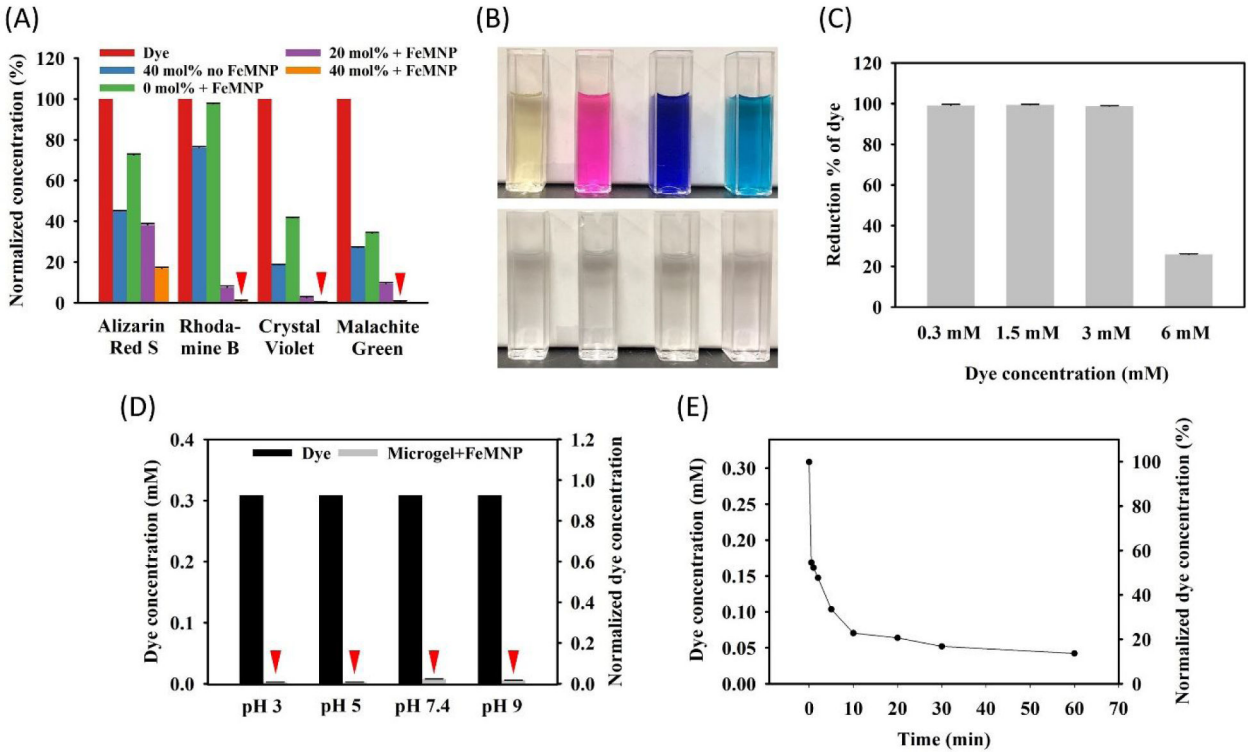

Figure 3.

(A) Normalized concentration of dye after incubating with 0–40 mol% DMA microgels (25 mg/mL) and FeMNP (5 mg/mL) at pH 3 for 24 hours. The concentration was normalized to the starting dye concentration or 150 mg/mL. (B) Photographs of dye solutions before (top row) and after (after row) incubation with microgels and FeMNP. (C) Percent Rhodamine B reduction for different starting concentrations of dye and incubated with 40 mol% DMA microgel (25 mg/mL) and FeMNP (5 mg/mL). (D) Reduction of Rhodamine B concentration at different pH for dye alone (■) and in the presence of 40 mol% DMA microgel (25 mg/mL) and FeMNP (5 mg/mL) (■) after 24-hour incubation, with a starting dye concentration of 0.3 mM. (E) Changes in the Rhodamine B concentration as a function of time during the incubation with 40 mol% DMA microgel (25 mg/mL) and FeMNP (5 mg/mL). Red triangles in figure are indicators for those extremely low data value.

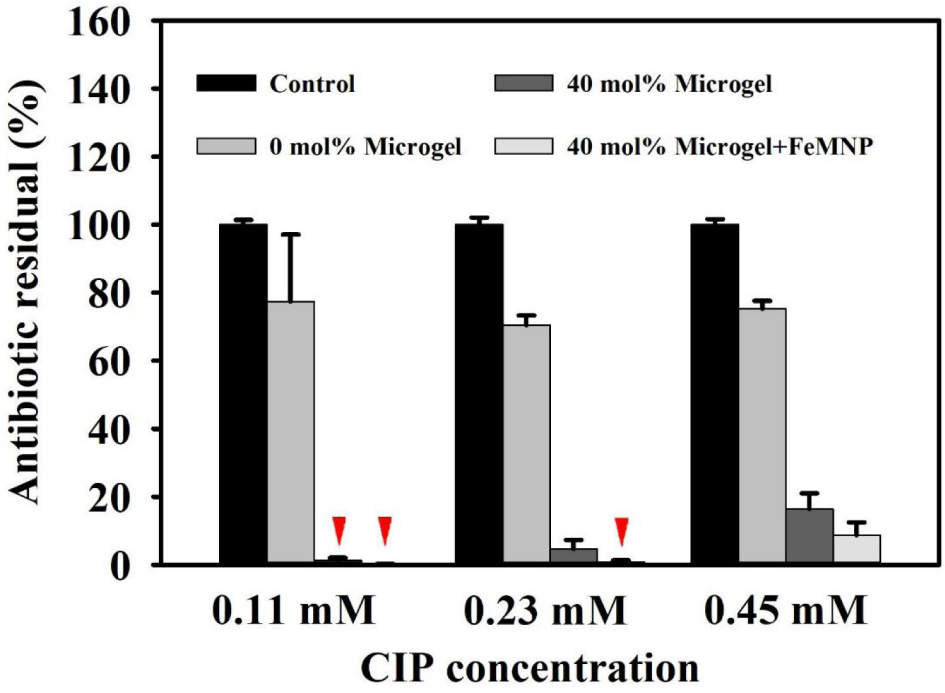

Figure 4.

Residual of the antibiotic, CIP, with different starting concentrations (0.11 to 0.45 mM) in PBS buffer (pH 7.4) after incubating with 40% DMA microgel (25 mg/mL) with and without FeMNP (5 mg/mL) for 24 hours. The control contains only CIP. Red triangles indicate extremely low values for a given treatment.

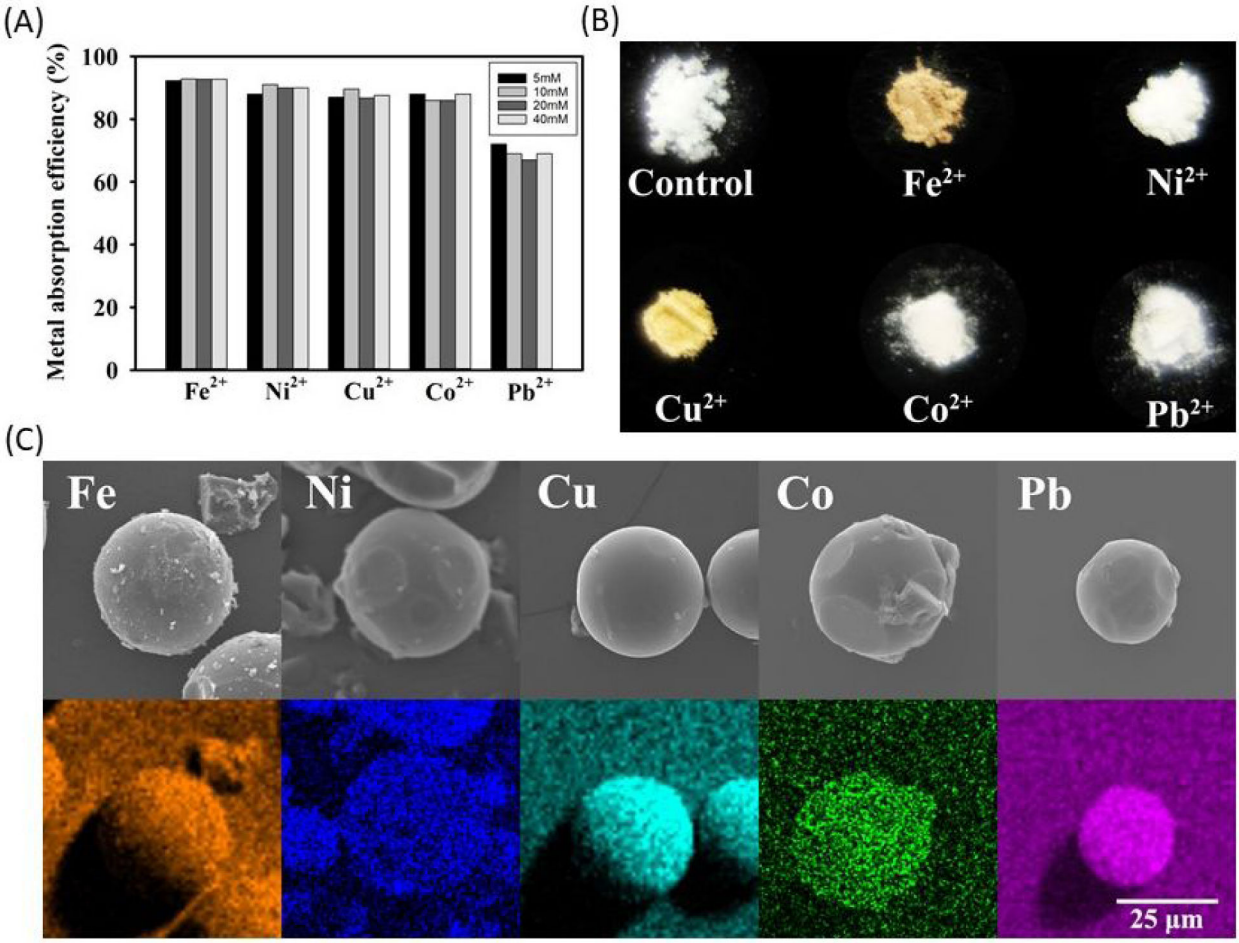

Figure 5.

(A) Percent removal of metal ions after incubating 40% DMA microgel (25 mg/mL) with a solution containing 5–40 mM of different metal ions as determined using ICP-OES. (B) Photograph of DMA microgels after absorbing the different metal ions. (C) SEM images (top row) and EDS mapping (bottom row) of microgels after metal ion absorption.

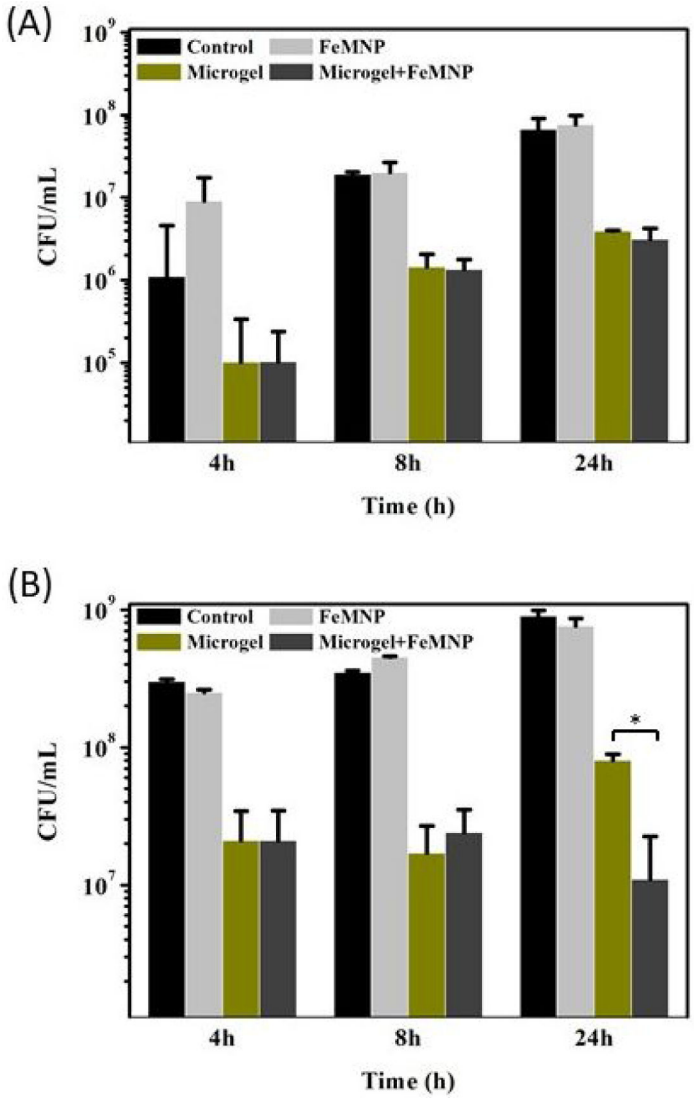

Figure 6.

Bacteria concentration of (A) *S. aureus* and (B) *E. coli* after incubating with FeMNP (2 mg/ mL), 40 mol% DMA microgel (10 mg/ mL), or the combination of the two for 4, 8, and 24 hours. The untreated control was the bacteria incubated in broth over the same periods. *p<0.05 when compared between two groups.

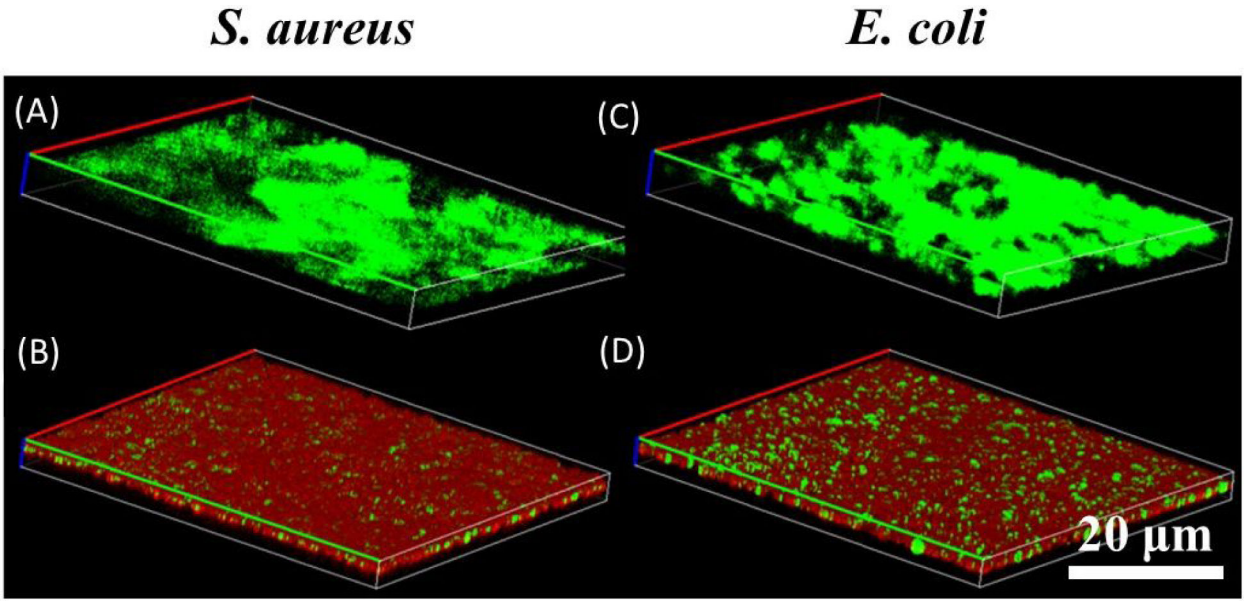

Figure 7.

LIVE/DEAD fluorescence images of *S. aureus* (A and B) and *E. coli* (C and D) after 24-hour incubation at 37 °C and pH 7.4 in the absence of (A and C) and in the presence of (B and D) 40 mol% DMA microgels (25 mg/mL) and FeMNP (5 mg/mL). Live and dead bacteria are stained green and red, respectively.

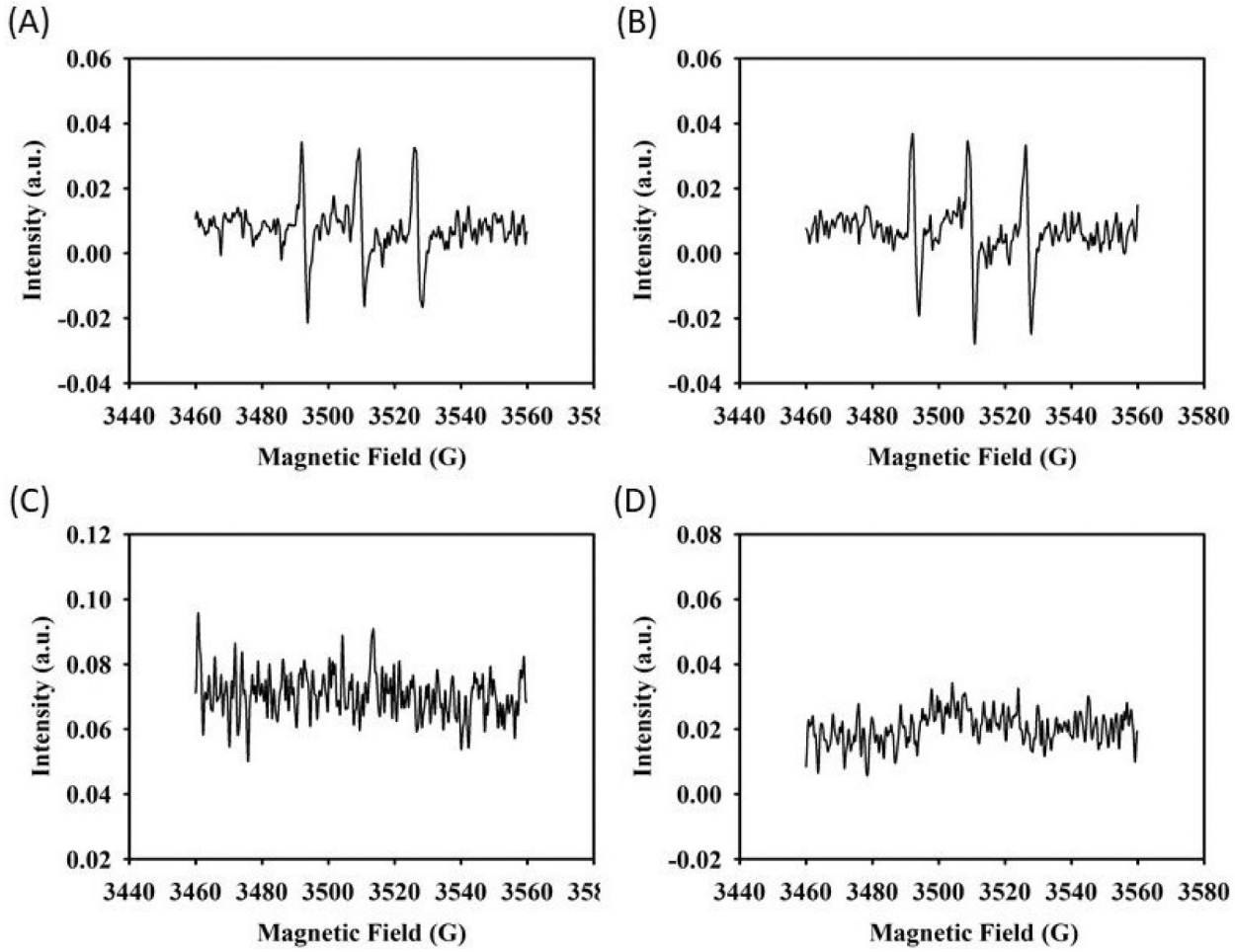

Figure 8.

EPR spectra of 40 mol% DMA microgel (25 mg/mL) and FeMNP (5 mg/mL) for the detection of $^1O_2$ in the presence of TEMP at (A) pH 3 and (B) pH 7.4 and $O_2{\cdot}^-$ and ·OH in the presence of DMPO at (C) pH 3 and (D) pH 7.4.

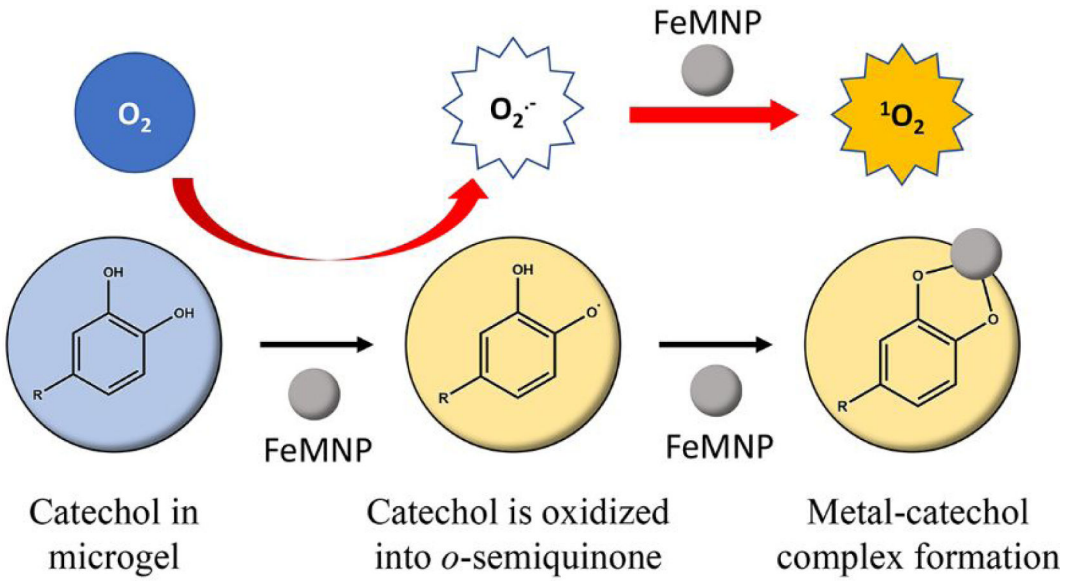

Figure 9.

Free radical generation mechanism of dopamine methacrylamide (DMA) microgel and iron magnetic nanoparticle (FeMNP). Catechol in DMA microgel was firstly oxidized into o-semiquinone. The electron transfer during this process converted molecular oxygen (O_2) into superoxide radical ($O_2 \cdot^-$). *o*-semiquinone was stabilized by forming metal-catechol coordination bond with FeMNP, resulting in the electron transfer of the superoxide radical on the highly reactive FeMNP surface and converting it to singlet oxygen.

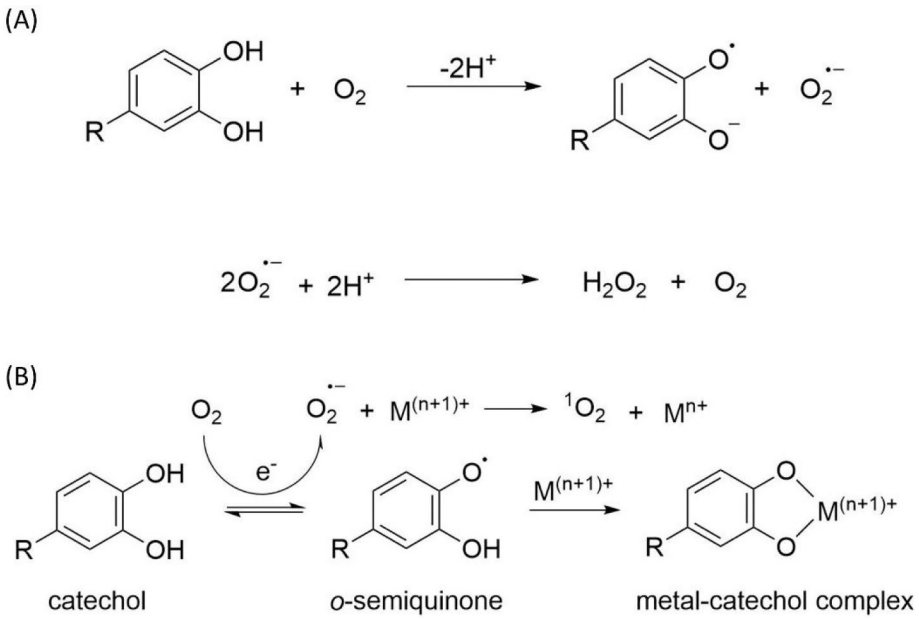

Scheme 1.

(A) During autoxidation, catechol is oxidized to quinone and superoxide radical ($O_2\cdot^-$) is generated as a byproduct. $O_2\cdot^-$ can be further converted to the more stable hydrogen peroxide (H_2O_2). (B) During metal ion-mediated oxidation, $O_2\cdot^-$ is generated when catechol is oxidized to *o*-semiquinone, which subsequently forms metal ion-catechol complex. $O_2\cdot^-$ can be further oxidized into singlet oxygen ($^1O_2$) by the metal ion.

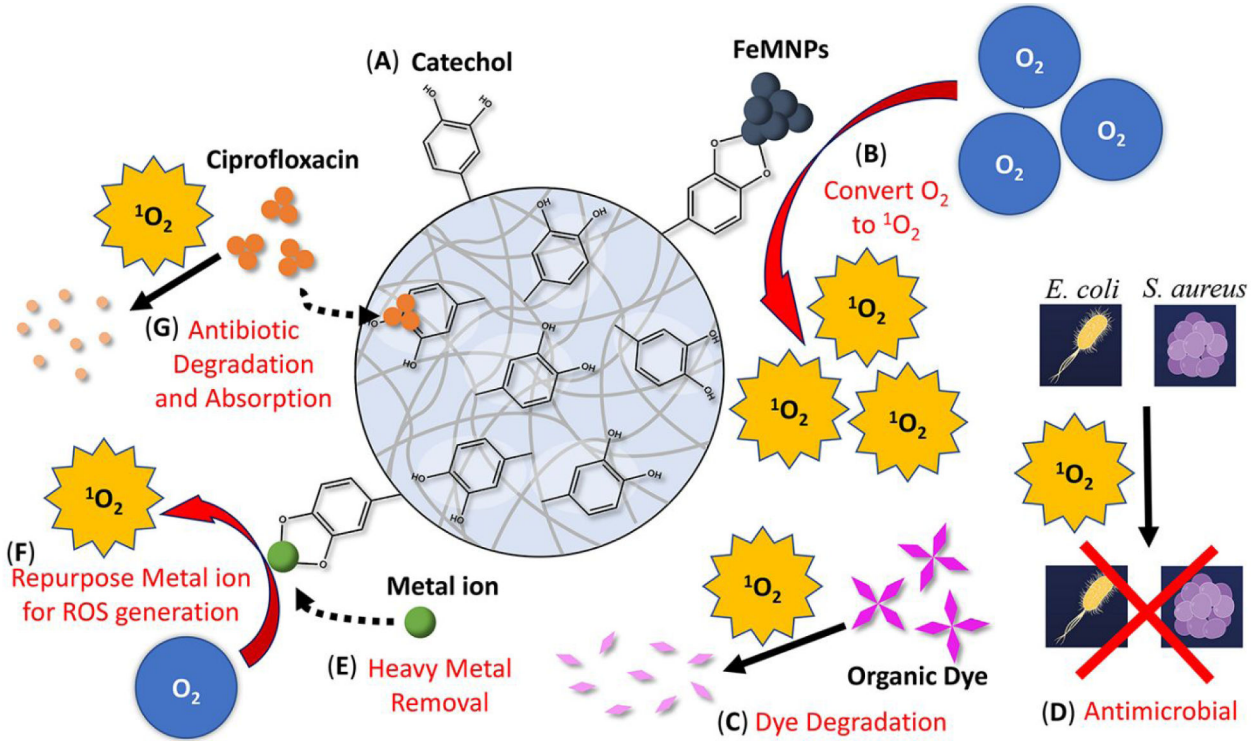

Scheme 2.

Schematic of the multifunctional DMA-containing microgel with the ability to generated ROS. (A) This microgel contains unoxidized catechol moiety. (B) In the presence of FeMNP, FeMNP-induced catechol oxidation converts molecular oxygen (O_2) into singlet oxygen ($^1O_2$), which can (C) degrades organic dyes, (D) kills bacteria such as *E. coli* and *S. aureus*. (E) Catechol can chelate metal ion and remove heavy metal from the solution and (F) repurpose the metal ion for ROS generation. (G) The microgel can absorb or degrade antibiotic drugs such as ciprofloxacin.